Journal of Chromatography B 1263 (2025) 124671

Contents lists available at ScienceDirect

Journal of Chromatography B

journal homepage: www.elsevier.com/locate/jchromb

Xiaojianzhong decoction inhibits gastric cancer progression and enhances 5-Fu efficacy by regulating the MAPK and PI3K-AKT signaling pathway

Yanxue Xu [a,1], Yumeng Zhang [a,1], Chen Huang [a], Min Zhao [a,**], Yihe Huang [b,*]

[a] School of Pharmacy, Shenyang Pharmaceutical University, Wenhua Road 103, Shenyang, Liaoning Province, China
[b] School of Public Health, Shenyang Medical College, Huanghe North Street 146, Shenyang, Liaoning Province, China

ARTICLE INFO

Keywords:
Xiaojianzhong decoction
Pharmacological mechanisms
Gastric cancer
Network pharmacology
In vitro validation
Experimental verification

ABSTRACT

Aim of the study: This study aims to investigate the pharmacological mechanisms underlying the enhancement of fluorouracil (5-Fu) efficacy by Xiaojianzhong decoction (XJZD) in the treatment of gastric cancer (GC).
Materials and methods: Network pharmacology was utilized to assess the therapeutic pathways of XJZD in the treatment of GC. The results from the network pharmacology analysis were validated through MTT assays, flow cytometry, qPCR, and ELISA experiments. Additionally, metabolomics was applied to identify differential metabolites and clarify the primary metabolic pathways involved.
Results: XJZD inhibited the proliferation of GC-803 cells and induced apoptosis. Furthermore, the combination of XJZD with 5-Fu significantly upregulated the mRNA levels of JNK1, JNK2, while downregulating the mRNA levels of ERK1, ERK2 and p38. Additionally, XJZD +5-Fu treatment reduced the expression of PI3K, AKT, and mTOR in GC-803 cells, suggesting that XJZD enhances the therapeutic effect of 5-Fu by inducing apoptosis and modulating the MAPK and PI3K-AKT signaling pathways. Metabolomics analysis identified 16 key metabolites that primarily influence amino acid and energy metabolism.
Conclusions: In this study, the potential therapeutic pathway of XJZD in combination with 5-Fu for the treatment of GC was identified through network pharmacology, in vitro validation, and metabolomics. The therapeutic mechanism of XJZD in GC involves the synergistic effects of multiple active ingredients, targets, and signaling pathways, as well as the modulation of amino acid and energy metabolism. These findings provide new insights into the pharmacological mechanisms underlying the combination of XJZD and 5-Fu in the treatment of GC.

1. Introduction

Gastric cancer (GC) is one of the most prevalent malignancies and a leading cause of cancer-related mortality worldwide. Common treatment modalities include surgery, radiation therapy, and chemotherapy [1]. While chemotherapy is a standard treatment option for GC, it is associated with significant side effects and the potential for the development of drug resistance [2]. Gastric Cancer Cells (GC-803) are cells commonly used in gastric cancer research , it is a well-established human gastric carcinoma cell line that is widely used in gastric cancer research [3]. For thousands of years, traditional Chinese medicine (TCM) has been utilized to treat GC by regulating the body's condition, thereby influencing the progression of the disease [4]. Moreover, TCM can help alleviate the side effects induced by radiotherapy and chemotherapy [5]. Xiaojianzhong decoction (XJZD) is a well-known herbal remedy in traditional Chinese medicine, consisting of Cmnamomi Mmulus (GZ), Radix Paeoniae Alba (BS), Glycyrrhizae Radix et Rhizoma (GA), Jujubae Fructus (DZ), Zingiberis Rhizoma Recens (SJ), and Yitang (YT). It has been used for over 2000 years to treat gastrointestinal disorders [6]. XJZD is commonly used in the treatment of gastrointestinal diseases. Modern pharmacological studies have shown that this formula possesses multiple pharmacological effects, including anti-inflammatory activity, enhancement of immune function, protection against lipid peroxidation damage, and regulation of cyclic nucleotide imbalance [41]. At present, there are few reports on the combined use of XJZD and 5-fluorouracil (5-Fu) to enhance the antitumor effect of 5-Fu, and the underlying mechanisms have not been thoroughly investigated. XJZD targets multiple molecular pathways involved in the progression of Gastrointestinal disorders, such as bile acid metabolism and the p62/Keap1/Nrf2 signaling pathway [7], and has demonstrated significant

* Corresponding author at: School of Public Health, Shenyang Medical College, Huanghe North Street 146, Shenyang, Liaoning Province, China.
** Corresponding author at: School of Pharmacy, Shenyang Pharmaceutical University, No. 103 Wenhua Road, Shenyang 110016, Liaoning Province, China.
[1] Yanxue Xu and Yumeng Zhang contributed equally

https://doi.org/10.1016/j.jchromb.2025.124671
Received 28 March 2025; Received in revised form 21 May 2025; Accepted 22 May 2025
Available online 26 May 2025
1570-0232/© 2025 Elsevier B.V. All rights are reserved, including those for text and data mining, AI training, and similar technologies.

clinical efficacy in previous studies. Cmnamomi Mmulus has been shown to suppress the autophagy of gastric mucosal cells [8], inhibit the replication of *Helicobacter pylori* (Hp), and possess anti-inflammatory and analgesic properties [9], Glycyrrhizae Radix et Rhizoma exhibits a range of biological functions, including anti-inflammatory, anti-hepatotoxic, immune-regulatory, antiviral, and anticancer activities [10], Jujubae Fructus polysaccharides promote tissue healing, modulate gut microbiota to provide anti-inflammatory benefits, support gastrointestinal health, and inhibit the proliferation of various cancer cell lines [11], Radix Paeoniae Alba regulates immune activity, acts as an antioxidant, and suppresses glycolysis [12], Zingiberis Rhizoma Recens may mitigate gastrointestinal side effects induced by cancer chemotherapy [13], alleviate oxidative stress and inflammation associated with GC, reduce GC cell activity, and inhibit tumor proliferation [14], lastly, Yitang treats chronic atrophic gastritis by modulating energy metabolism, gastric emptying, and alterations in the gut microbiome [15]. Network pharmacology is an approach that utilizes biological networks to comprehensively elucidate the complex interactions among biological systems [16], medications, and diseases, thereby shedding light on the intricate mechanisms of drug action [17]. This approach provides a theoretical foundation for further research on traditional Chinese medicine [18]. Metabolomics is a powerful technique for analyzing the composition of metabolites and their alterations in various biological samples [19]. It is widely used in studying disease biomarkers and drug mechanisms of action, providing comprehensive and accurate analyses of metabolites that facilitates in-depth exploration of metabolic changes in organisms [20]. In this study, we investigated the mechanism of action of XJZD in GC using network pharmacology, and validated the pharmacodynamic effects of XJZD in combination with 5-Fu through in vitro experiments. We hypothesize that the combination of herbs XJZD and 5-Fu exerts synergistic anti-GC effects by modulating the PI3K/AKT, MAPK signaling pathway. The primary intracellular metabolic pathways influenced by XJZD were identified through non-targeted metabolomics.

2. Methods

2.1. Chemicals and reagents

The ingredients used in this study included *Cmnamomi Mmulus* (dried shoots of *Cinnamomum cassia Presl*, Guizhi; batch number: 240101991; source: Guangdong, China), *Radix Paeoniae Alba* (dried roots of *Paeonia lactiflora* Pall, Baishao; batch number: 240300239; source: Anhui, China), *Jujubae Fructus* (dried ripe fruit of *Ziziphus jujuba* Mill, Dazao; batch number: 231150417; source: Xinjiang, China), *Glycyrrhizae Radix et Rhizoma* (dried roots and rhizomes of *Glycyrrhiza uralensis* Fisch., *Glycyrrhiza inflata* Bat., or *Glycyrrhiza glabra* L., Gancao; batch number: 231102871; source: Neimenggu, China), *Zingiberis Rhizoma Recens* (fresh rhizomes of *Zingiber officinale* Rosc, Shengjiang; commercially available; source: Liaoning, China), and Yitang (Yitang; batch number: 20240102; source: Hebei, China). These ingredients were obtained from Guoda Pharmacy (Shenyang, China). All crude drugs were ground into powder, and the XJZD was prepared by placing the Chinese herbs in a decoction pan according to the proportions of ancient recipes: Cmnamomi Mmulus (9 g), Radix Paeoniae Alba (18 g), Jujubae Fructus (30 g), Glycyrrhizae Radix et Rhizoma (6 g), Zingiberis Rhizoma Recens (9 g), and Yitang (30 g). After adding 300 mL of water, the residue was discarded, and the mixture was steamed and freeze-dried. Fluorouracil (5-Fu) was purchased from Shanghai Adamas Technology Co. Ltd. (Lot: P2082288). Methylthiazolyldiphenyl-tetrazolium bromide (MTT), Annexin V-FITC/PI Apoptosis Assay Kit, propidium iodide (PI), and penicillin-streptomycin solution (100×) were acquired from Beyotime Institute of Biotechnology (Shanghai, China).

2.2. Data sources of network pharmacology

2.2.1. Acquisition and processing of XJZD

The active components and their associated protein targets of the six ingredients of XJZD were obtained through the Traditional Chinese Medicine Systems Pharmacology (TCMSP) platform (https://old.tcmsp-e.com/tcmsp.php). The screening criteria included an Oral Bioavailability (OB) $\geq$ 30 % and a Drug Likeness (DL) $\geq$ 0.18. Based on these parameters, the active ingredients and their corresponding protein targets were determined. The protein targets were then mapped to their official gene names using the UniProt database (https://www.uniprot.org/).

2.2.2. Identification of GC-related gene targets

Genes associated with gastric cancer (GC) were collected by searching for "gastric cancer" in multiple databases. In the GeneCards database (https://www.genecards.org/), a correlation score of $\geq$1.0 was used as the screening criterion. In the DisGeNET database (https://disgenet.org/), a correlation score of $\geq$0.1 was applied. The results from the PharmTDD database (https://db.idrblab.net/ttd/) and the OMIM database (https://www.omim.org/) were also incorporated. Duplicate gene targets were removed. A Venn diagram was constructed to analyze the overlapping genes. This approach enabled the identification of potential targets of XJZD for the treatment of GC.

2.2.3. Protein-protein interaction (PPI) network construction

The overlapping genes were uploaded to the STRING database (https://string-db.org/) to construct the PPI network. "*Homo sapiens*" was selected as the organism, and the settings were adjusted to "highest confidence" (>0.9). Additionally, the option to "hide disconnected nodes in the network" was enabled. All other parameters were set to their default values. The resulting network was analyzed using Cytoscape 3.9.1, which facilitated the visualization of complex gene relationships. The CytoNCA plug-in was employed for network topology analysis, and the colors and sizes of nodes and edges were adjusted according to the Degree values.

2.2.4. Construction of active ingredient-target network

The active ingredients and their corresponding intersecting targets were imported into Cytoscape 3.9.1 to construct the "active ingredient-target" network. The degree values of the active ingredients and targets were analyzed, and interactions between them were represented by edges connecting the ingredients and their respective targets.

2.2.5. Enrichment analysis

The Metascape database (https://metascape.org/gp/index.html) was used to perform enrichment analysis on the 29 targets from the PPI network with betweenness centrality values above the median. Gene Ontology (GO) enrichment and Kyoto Encyclopedia of Genes and Genomes (KEGG) pathway enrichment analyses were conducted. GO enrichment included biological processes, cellular components, and molecular functions. The GO enrichment analysis was performed using a significance threshold of $P < 0.01$. Both GO enrichment and KEGG pathway analyses were organized based on the number of enriched genes, and the top 20 pathways were displayed.

2.2.6. Molecular docking technology

The five most important protein targets identified in the PPI network were selected for molecular docking with their corresponding compounds. The chemical components were downloaded in 3D .sdf format, refined using Chem3D, and stored in .mol2 format. The 3D structures of the target proteins were obtained from the RCSB PDB database (https://www.rcsb.org/). Using PyMOL (http://www.pymol.org/pymol), water and solvent molecules were removed, and hydrogen atoms were added to the core targets. The processed structures were saved in .pdbqt format. Hydrogen atoms were added to the chemical structures using

AutoDockTools (https://ccsb.scripps.edu/mgltools/downloads/), and the final structures were also saved in .pdbqt format. Docking simulations were carried out using AutoDock Vina 1.2.3 (https://vina.scripps.edu/), generating binding energy results for each of the eight compounds docked with the five targets. The docking results were visualized using PyMOL and the images were saved for further analysis.

2.2.7. Validation of key targets in GEPIA, HPA and DriverDBv3 database

The expression levels of 11 key targets in GC (TCGA-STAD) were validated using the GEPIA online tool (http://gepia.cancer-pku.cn/index.html). Protein expression levels and their distribution in both normal stomach and GC tissues were retrieved from the Human Protein Atlas (HPA) database (https://www.proteinatlas.org/). Survival data for the 11 key genes were accessed through the DriverDBv3 database (http://driverdb.tms.cmu.edu.tw/).

2.3. Experimental verification in vitro

2.3.1. Cell culture

GC-803 cells were cultured in RPMI-1640 medium supplemented with 10 % fetal bovine serum and 1 % penicillin-streptomycin solution. The cells were maintained in a humidified incubator at 37 °C with 5 % CO_2. The medium was replaced every 2–3 days. Once the cells reached 90 % confluence, they were digested and passaged.

2.3.2. Cell viability test (MTT assay)

Cells were divided into groups, and XJZD was added at final concentrations of 3, 4.5, 6, 7.5, and 9 mg/mL, while 5-Fu was applied at concentrations of 0.39, 1.56, 6.25, 25, and 100 μg/mL. XJZD and 5-Fu were used in combination with a 1:1 correspondence of concentrations. After 48 h of incubation, the 96-well plates were removed, the medium was discarded, and 10 μL of MTT solution was added to each well. The plates were then incubated at 37 °C in a 5 % CO_2 incubator for 4 h. Following this, 200 μL of DMSO was added to each well, and the plates were shaken for 10 min at room temperature. The absorbance at 450 nm (optical density) was assessed using a microplate reader, The entire experiment was repeated five time.

2.3.3. Assessment of apoptosis using flow cytometry

The cells were divided into three groups: 5-Fu group (5-Fu), traditional Chinese medicine group (XJZD), and combined treatment group (5-Fu + XJZD). In the XJZD group, the final concentration of XJZD was 3 mg/mL, in the 5-Fu group, the concentration of 5-Fu was 6.25 μg/mL, and in the combined group, the final concentrations were 3 mg/mL for XJZD and 6.25 μg/mL for 5-Fu. Cells were seeded into 6-well plates and incubated at 37 °C with 5 % CO_2 for 12 h. After the drugs were added to their respective groups, the cells were further incubated for 24 h under the same conditions.

Following incubation, the supernatant was collected into centrifuge tubes. Each well was then treated with 1 mL of trypsin digestion solution (without EDTA), and the cells were centrifuged at 4 °C for 5 min at 1500 rpm. The cell pellet was washed with pre-chilled PBS and centrifuged again. After removing the supernatant, 100 μL of binding buffer was added to each group, followed by 5 μL of Annexin V-FITC and 10 μL of propidium iodide (PI). The samples were protected from light and incubated at room temperature (25 °C) for 15 min. After incubation, 100 μL of binding buffer was added to each group and mixed thoroughly. The samples were then analyzed using flow cytometry within 1 h. The experiment was repeated three times.

2.3.4. mRNA expression analysis of ERK, P38, and JNK using qPCR

Total RNA was extracted from cells using an RNA extraction kit (Vazyme, Nanjing, China). Residual genomic DNA was eliminated, and reverse transcription was performed using HiScript III RT SuperMix (Vazyme, Nanjing, China) to synthesize complementary DNA (cDNA) from RNA. Real-time quantitative PCR was then conducted using ChamQ Universal SYBR qPCR Master Mix (Vazyme, Nanjing, China) to amplify the cDNA with fluorescence detection. The experiment was repeated three times. Relative gene expression was calculated using the 2ˆ-ΔΔCT method, with the target gene's Ct value normalized to that of the internal reference gene (GAPDH). The primer sequences used were as follows:

GAPDH: F-5′-GATTCCACCCATGGCAAATTC, R-5′-CTGGAAGATGGTGATGGGATT;

JNK1: F-5′-CCGTCTCCTTTAGCACAGGT, R-5′-TGTATCCGAGGCCAAAGTCG;

JNK2: F-5′-TCCAAGGCACTGACCATATTGA, R-5′-TCCTCACAGTTGGCTGAAGT;

p38: F-5′-ATGCCAAGCCATGAGGCAA, R-5′-GCATCTTCTCCAGCAAGTCG;

ERK1: F-5′-ACCACATTCTGGGCATCCTG, R-5′-CCGTCGGGTCATAGTACTGC;

ERK2: F-5′-GCCGAAGCACCATTCAAGTT, R-5′-CCTCTGAGCCCTTGTCCTGA.

2.3.5. Enzyme-linked immunosorbent assay (ELISA)

The levels of PI3K, AKT, and mTOR in the cells were quantified using an ELISA kit (Meimian Biotechnology, Jiangsu, China) according to the manufacturer's instructions. Results were calculated as the average of five parallel experiments.

2.3.6. UHPLC-MS metabolomics analysis

After 48 h of cell treatment, the culture medium was completely aspirated from the petri dish. To digest the cells, 1 mL of trypsin was added and incubated for 5 min. The cells were then dispersed by gentle pipetting, and 3 mL of culture medium was added to terminate the digestion. The cell suspension was transferred to a new 15 mL centrifuge tube and centrifuged at 4 °C for 5 min at 1000 rpm. The supernatant was discarded, and the cells were washed three times with 5 mL of PBS. Approximately 2×10^6 cells were collected per sample. The collected cells were mixed with 1 mL methanol-water (4:1, *v*/v), subjected to three freeze-thaw cycles in liquid nitrogen (3 min each), and disrupted using a cell homogenizer to extract intracellular metabolites. The suspension was then centrifuged at 4 °C, 12,000 rpm for 10 min, and the supernatant was collected. The remaining cell pellet was re-extracted by adding 1 mL of methanol-water (4:1, v/v), mixed, and subjected to the same extraction process twice. The combined supernatants were transferred to a 5 mL centrifuge tube and evaporated under a nitrogen stream at room temperature. For each group, six samples were prepared in parallel and stored at −80 °C. The samples were then redissolved in 100 μL acetonitrile-water (85:15, v/v), vortexed for 1 min, sonicated for 1 min, and centrifuged at 13,000 rpm for 20 min. Finally, 80 μL of the supernatant was transferred to the injection vial for UHPLC-MS analysis.

UHPLC-MS analysis was conducted using the Waters ACQUITY UPLC system (Agilent, USA). A Kromat Universil XB C18 column (150 mm × 2.1 mm, 3 μm) was used for chromatographic separation. The flow rate was set to 0.2 mL/min, and the column temperature was maintained at 35 °C. The mobile phase consisted of 0.1 % (*v*/v) formic acid in water (Phase A) and 0.1 % (v/v) formic acid in acetonitrile (Phase B). The elution procedure is outlined below:

Time(min)	B(%)
0	95
2	75
4	45
8	15
10	95
13	95

The analysis was performed using an electrospray ionization (ESI) source in both positive and negative ion detection modes. The *m/z* scan range was set from 100 to 1000 Da for full scans. The following settings

were configured: cone voltage of 35 V; capillary voltage of 3.2 kV; desolvation temperature at 350 °C; source temperature at 120 °C; desolvation flow rate of 600 L/h; cone gas flow rate of 50 L/h; and collision energy ranging from 10 to 30 eV.

2.3.7. Methodological review

A 5 μL aliquot from each group sample was pooled to prepare the quality control (QC) samples. For methodological evaluation, the retention times (tR) and the corresponding corrected peak areas (Area) of six representative characteristic ions in the chromatogram were selected. Method repeatability, system stability, sample pretreatment stability, and freeze-thaw stability were assessed by calculating the relative standard deviation (RSD) of the corrected peak areas.

2.3.8. Statistical analysis

The experimental results are presented as mean ± standard deviation. GraphPad Prism (version 8.0) was used for plotting. A p-value of <0.05 was considered significant, <0.01 was considered very significant, and < 0.001 was considered extremely significant.

LC-MS data files were converted to ABF format using the Analysis Base File Converter software. The converted data were then imported into MS-DIAL software, where the retention time was set to 13 min, and

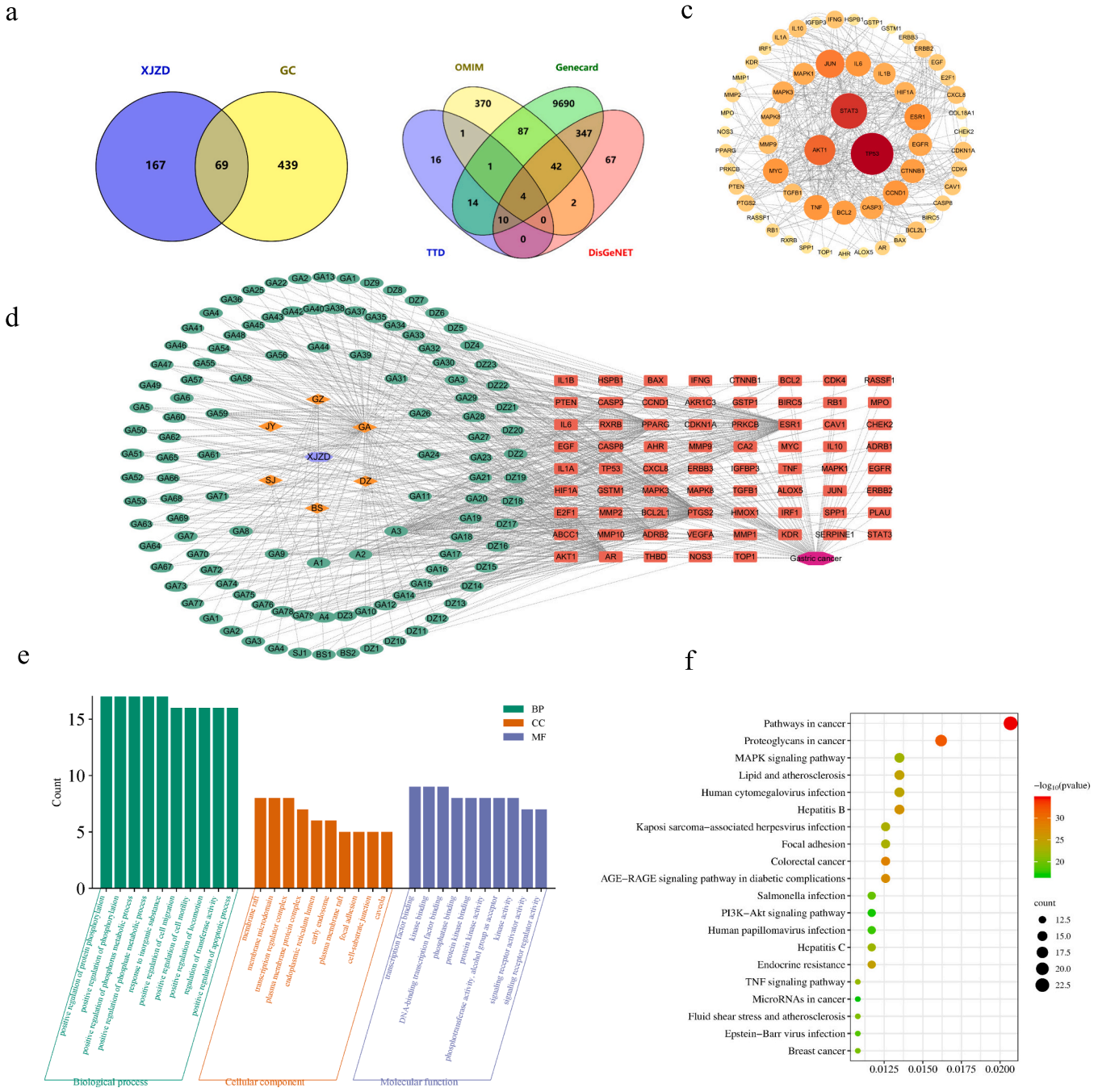

Fig. 1. Target collection and network construction. a) Venn diagram of XJZD component targets and GC targets. b) GC-related targets. c) Cytoscape treated PPI network of XJZD tre ated GC. d) "active ingredient-target" network. e) GO enrichment analysis of XJZD in treatment of GC. f) KEGG pathways enrichment analysis of XJZD in treatment of GC.

the *m/z* range was set to 10–1000 Da. After normalization, the data were imported into SIMCA software for PCA and OPLS-DA multivariate statistical analysis. In the OPLS-DA analysis, variables with VIP > 1.0 and p-value <0.05 were considered significant thresholds for screening potential biomarkers with meaningful differences.

The results were analyzed using the MS-DIAL database (http://prime.psc.riken.jp/compms/msdial/main.html#MSP), in combination with relevant literature and other available databases, such as HMDB (http://www.hmdb.ca), MassBank (http://www.massbank.jp), and KEGG (http://www.genome.jp), for biomarker identification.

3. Results

3.1. Target prediction of XJZD for GC

Using the TCMSP database and following the selected criteria, 101 active components of XJZD were identified. These included 4 compounds in GZ, 2 in BS, 79 in GA, 11 in DZ, 1 in SJ, and 4 shared components found in two or more of the traditional Chinese medicines. The ingredient details were standardized using the UniProt database, with the species selected as "*Homo sapiens*." After removing duplicates and invalid entries, a total of 236 ingredient targets were obtained. Combining these targets with GC targets from four disease databases led to the identification of 508 targets (Fig. 1a). The Venn diagram (Fig. 1b) highlights that there are 69 potential targets shared between XJZD and GC.

3.2. PPI network construction and key targets screening

After submitting all anticipated target genes to the STRING database, a high-confidence threshold of 0.9 was applied for analysis. The protein-protein interaction (PPI) network, consisting of 69 nodes and 231 edges, was created using Cytoscape (version 3.9.1). In this network, nodes represent different targets, while edges indicate interactions between them. The size and color depth of the nodes reflect their degree values (Fig. 1c) (Table 1). The network's topological parameters were assessed using the Network Analyzer tool. Among the targets, the top 11 based on degree were as follows:

TP53 (degree = 62), STAT3 (degree = 50), AKT1 (degree = 40), JUN (degree = 36), ESR1 (degree = 32), IL6 (degree = 30), MYC (degree = 30), TNF (degree = 30), CCND1 (degree = 30), CTNNB1 (degree = 28), BCL2 (degree = 28). These results highlight the significant importance of these targets and the strong interconnections among them. Genes with higher degree values are likely to serve as promising therapeutic targets for treating GC with XJZD.

3.3. Active ingredient-target network analysis

The "active ingredient-target" network was constructed using Cytoscape version 3.9.1 (Fig. 1d). From the analysis of the network diagram, it is evident that XJZD interacts with a wide range of potential targets, playing a crucial role in the treatment of GC and other diseases (Table 2).

Table 1
Details regarding the top 11 targets based on their degree value.

Number	Degree	Name	BetweennessCentrality	ClosenessCentrality
1	62	TP53	0.27	0.61
2	50	STAT3	0.18	0.60
3	40	AKT1	0.08	0.56
4	36	JUN	0.08	0.54
5	32	ESR1	0.05	0.52
6	30	IL6	0.06	0.50
7	30	MYC	0.02	0.51
8	30	TNF	0.07	0.51
9	30	CCND1	0.06	0.50
10	28	CTNNB1	0.04	0.50
11	28	BCL2	0.01	0.50

3.4. GO enrichment and KEGG enrichment

The Metascape platform was used to investigate the signaling pathways of 29 targets with a betweenness centrality value greater than the median. A significance threshold of P < 0.01 was applied, leading to the identification of 1043 significant Gene Ontology (GO) entries. These included 948 biological process (BP) entries, 59 molecular function (MF) entries, and 36 cellular component (CC) entries (Fig. 1e).

The KEGG pathway enrichment analysis identified 151 pathways, and the top 20 enriched pathways were visualized (Fig. 1f). According to the GO analysis, key biological processes included the response to inorganic compounds, enhancement of protein phosphorylation, positive regulation of phosphorylation, membrane raft formation, transcription regulator complex assembly, DNA-binding transcription factor binding, and kinase binding. KEGG pathway analysis indicated that the therapeutic effects of XJZD on GC are primarily associated with pathways such as proteoglycans in cancer, the MAPK signaling pathway, and Hepatitis B (Fig. 1f). The MAPK pathway is crucial in regulating cellular processes that lead to the malignant transformation of normal cells [21], additionally, the PI3K/AKT pathway plays a pivotal role in promoting tumor cell growth, cancerous transformation, and the inhibition of programmed cell death in cancer cells [22].

3.5. Results of molecular docking

A binding energy less than −5 kcal/mol indicates strong binding affinity. The top five core targets and their corresponding compounds (TP53 - quercetin, STAT3 - Licochalcone A, AKT1 - quercetin, AKT1 - kaempferol, AKT1 - beta-carotene, JUN - beta-sitosterol, ESR1 - naringenin, ESR1 - formononetin) were subjected to molecular docking using the Autodock Vina module. The docking analysis visualized the binding interactions and affinities between the active compounds and their core targets. The results revealed the interaction patterns, including the specific residues involved and the number of hydrogen bonds formed (Fig. 2). The strongest binding affinity was observed for the docking of beta-sitosterol with the core target JUN, with a minimum binding energy of −8.56 kcal/mol.

3.6. Validation of the key targets in GEPIA, HPA and DriverDBv3 database

The GEPIA database results showed that the mRNA expression levels of TP53, CCND1, MYC, and CTNNB1 were significantly higher in GC tissues compared to normal tissues (Fig. 3a). As illustrated in Fig. 3b, protein expression levels of JUN, MYC, and TNF were also elevated in GC tissues compared to normal gastric tissues. However, no significant differences in the expression of other genes were observed between GC and normal tissues. Furthermore, the DriverDBv3 database was utilized to analyze overall survival rates. The results indicated that higher expression levels of TP53, IL6, and ESR1 were significantly associated with lower survival rates ($P < 0.05$) (Fig. 3c).

3.7. Experimental verification in vitro

3.7.1. Cell viability test (MTT assay)

The toxic effect on GC-803 cells increased with higher concentrations, resulting in a progressive rise in cell inhibition. This effect was more pronounced with co-administration (Fig. 4a).

3.7.2. Evaluation of apoptosis by flow cytometry

The results of the apoptosis assay using Annexin V-FITC/PI double-staining showed that, compared to XJZD and 5-Fu administration alone, the combined administration significantly increased the apoptosis rate ($P < 0.05$) (Fig. 4b).

Table 2
Information of active ingredient.

Code name	CAS	Compound	Degree	BetweennessCentrality	ClosenessCentrality
A3	117–39-5	quercetin	56	0.20	0.55
A2	520–18-3	kaempferol	18	0.03	0.44
GC59	58,749–22-7	licochalcone a	13	0.02	0.42
A1	64,997–52-0	beta-sitosterol	12	0.02	0.44
GC11	480–41-1	naringenin	11	0.01	0.42
GC44	41,983–91–9	Glabranin	9	0.00	0.41
GC8	28,955–29-5	7-Methoxy-2-methyl isoflavone	7	0.00	0.41
GC9	485–72-3	formononetin	7	0.00	0.41
GC24	146,763–58-8	Glypallichalcone	7	0.00	0.41
GC26	58,749–23-8	Licochalcone B	7	0.00	0.41
GC31	124,596–86-7	Gancaonin B	7	0.00	0.41
GC39	157,414–04-5	shinpterocarpin	7	0.00	0.41
GC56	65,428–13-9	1-Methoxyphaseollidin	7	0.00	0.41
GC58	106,610–60-0	3'-Hydroxy-4'-O-Methylglabridin	7	0.00	0.41
GC61	–	2-[(3*R*)-8,8-dimethyl-3,4-dihydro-2H-pyrano[6,5-*f*]chromen-3-yl]-5-methoxyphenol	7	0.00	0.41
GC71	–	Licoagrocarpin	7	0.00	0.41

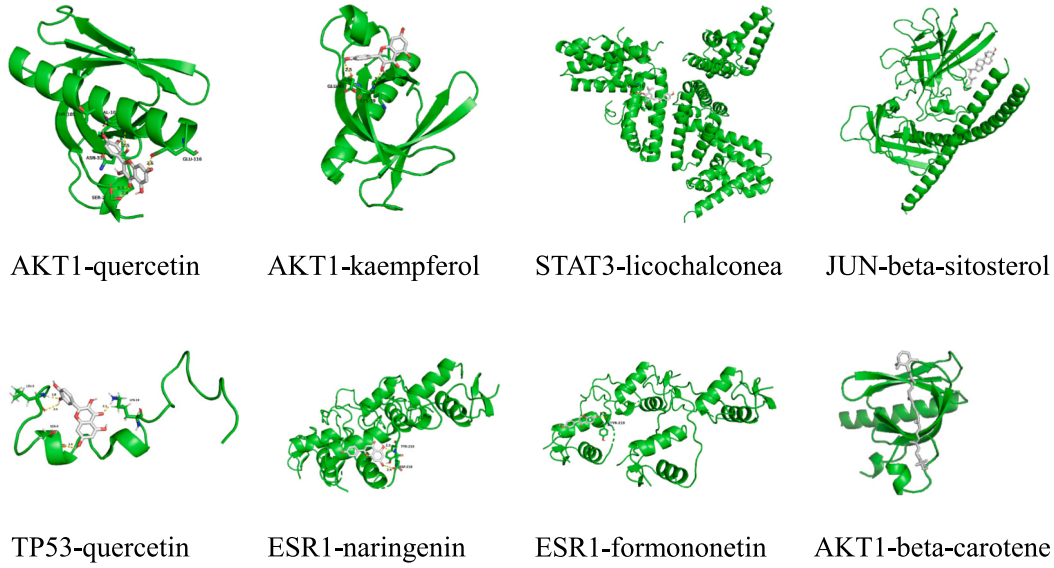

Fig. 2. Partial docking model and site map for the core targets of XJZD core targets and corresponding components.

3.7.3. The expression levels of ERK, p38 and JNK mRNA were detected by qPCR

qRT-PCR was used to assess the effects of XJZD, 5-Fu, and their combination on the mRNA expression of JNK1, JNK2, p38, ERK1, and ERK2. The mRNA expression levels of JNK1, JNK2 were higher in the XJZD combined with 5-Fu group than in the XJZD or 5-Fu alone groups ($P < 0.05$). Conversely, the mRNA expression levels of ERK1, ERK2 and p38 were lower in the XJZD combined with 5-Fu group than in the XJZD or 5-Fu groups ($P < 0.05$) (Fig. 4c).

3.7.4. Enzyme-linked immunosorbent assay

Enzyme-linked immunosorbent assay (ELISA) was used to measure the effects of XJZD, 5-Fu, and their combination on the expression of PI3K, AKT, and mTOR. The expression levels of PI3K, AKT, and mTOR were lower in the XJZD combined with 5-Fu group compared to the XJZD or 5-Fu alone groups (Fig. 4d).

3.7.5. Validation of LC-MS analytical methods

Method Repeatability: Six parallel QC samples were independently prepared and analyzed. The relative standard deviations (RSDs) of the retention times (tR) and corresponding peak areas were calculated to evaluate the repeatability of the method.

System Stability: A single QC sample was injected at regular intervals, specifically after every six sample injections. The RSDs of the tR and peak areas for six representative ions were calculated to assess the stability of the analytical system.

Pretreatment Stability: Six parallel QC samples were prepared and kept at 4 °C for 24 h. These were analyzed together with freshly prepared QC samples, and the RSDs of the tR and peak areas were calculated to evaluate the stability of the sample pretreatment process.

Freeze–Thaw Stability: Six parallel QC samples were subjected to three freeze–thaw cycles and then analyzed together with freshly prepared QC samples. The RSDs of the tR and peak areas were calculated to assess the stability of the samples after repeated freeze–thaw cycles.

In all methodological evaluations, the RSD values did not exceed ±15 %, indicating that the analytical method possesses good repeatability, stability, and applicability (Table 3).

3.7.6. Metabolomics profiling

The total ion chromatograms (TIC) of the cell samples are presented in Fig. 5. Principal Component Analysis (PCA) was initially employed to assess the grouping of the experimental cellular samples (Fig. 6a). Although some partial overlap was observed between the groups, the separation was generally distinct. Notably, the XJZD, 5-Fu, and XJZD+5-Fu combination groups were clearly separated from the GC group, indicating significant metabolic differences between the treated

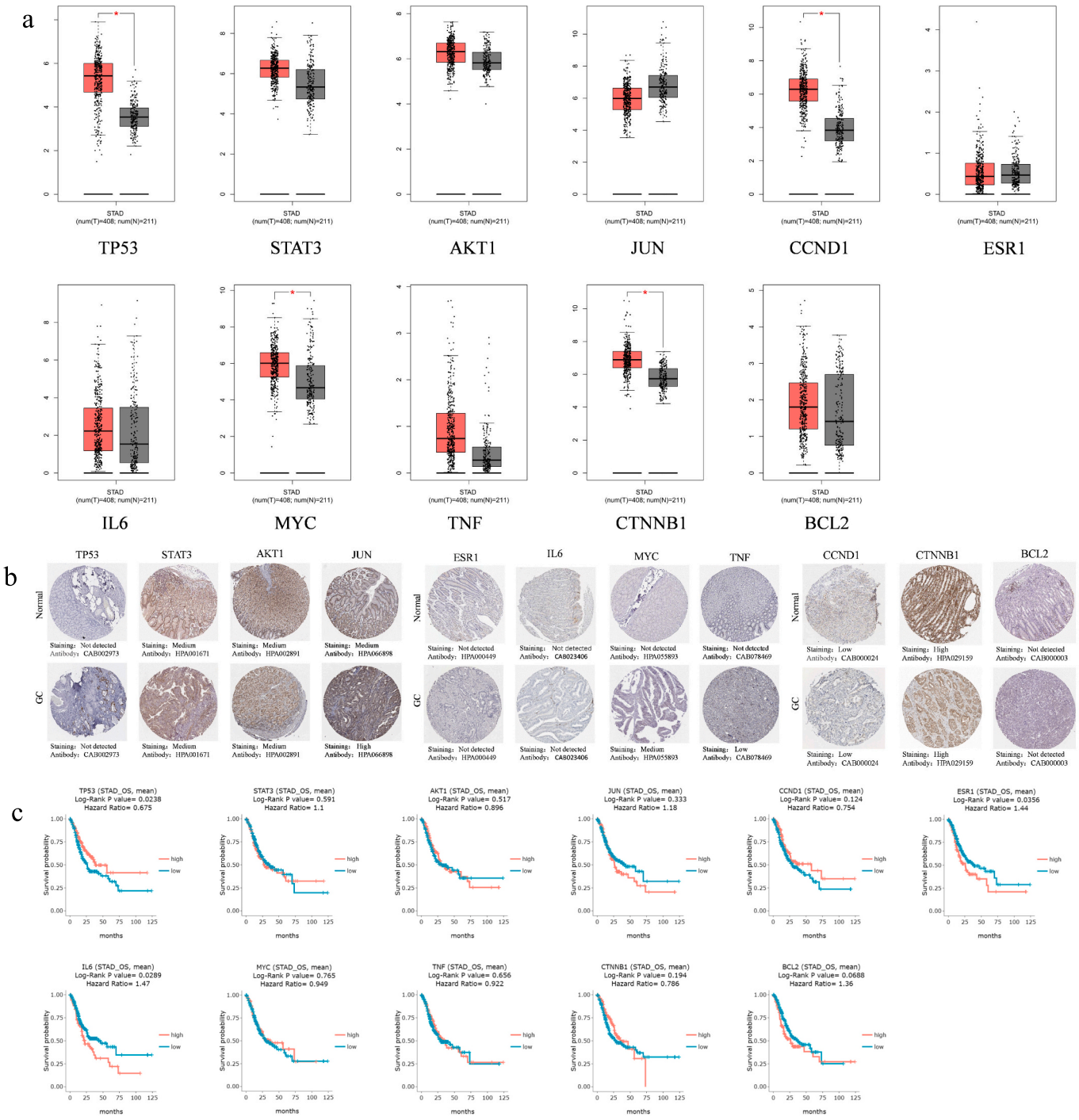

Fig. 3. a) The expression levels of hub genes in the GEPIA database. The red box plots indicate tumor samples, while the gray box plots represent normal samples. b) The protein levels of key genes in the HPA. c)The overall survival of hub genes in DriverDBv3 database. The blue indicates low levels of expression, while the red signifies high levels of expression. (For interpretation of the references to color in this figure legend, the reader is referred to the web version of this article.)

and GC groups. This suggests that the drug treatments had a measurable impact on the metabolism of GC-803 cells. Furthermore, clear distinctions were observed between the XJZD and 5-Fu groups and the XJZD+5-Fu group, suggesting that the mechanisms underlying the effects of XJZD, 5-Fu, and the XJZD+5-Fu combination on GC cell metabolism may differ.

To further elucidate the contribution of metabolites to the observed group differences and to identify potential metabolic biomarkers, multivariate statistical analyses were conducted using Orthogonal Partial Least Squares Discriminant Analysis (OPLS-DA) in supervised mode. OPLS-DA was applied to the metabolite data from each experimental group, and score plots were generated (Fig. 6b). The analysis revealed a clearer separation between the experimental groups under the OPLS-DA model, suggesting significant metabolic variations between them. The quality of the OPLS-DA model was assessed using the parameters R^2Y and Q^2. R^2Y indicates the goodness of fit of the model, while Q^2 assesses its predictive power. A value of R^2Y and $Q^2 > 0.5$ is considered acceptable, with values closer to 1 indicating higher model accuracy and reliability. For the positive ion model, $R^2Y = 0.978$ and $Q^2 = 0.912$, and for the negative ion model, $R^2Y = 0.898$ and $Q^2 = 0.811$, indicating

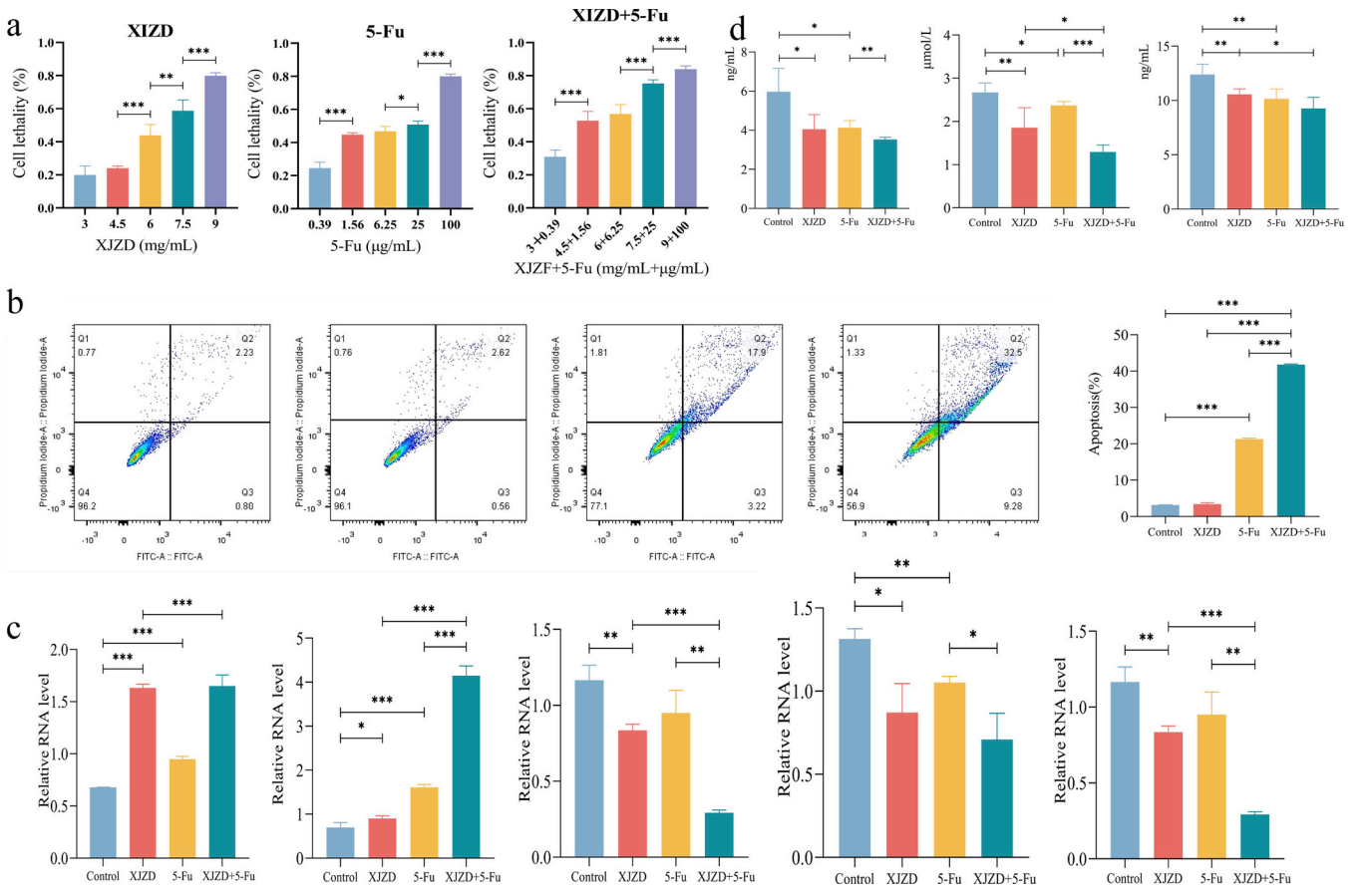

Fig. 4. a) Effect of different group on the activity of GC-803 cells. b) Effect of different group on apoptosis of GC-803 cells. c) qPCR was conducted to measure the expression levels of JNK1, JNK2, p38, ERK1and ERK2 mRNA across various groups. d) ELISA was conducted to measure the expression levels of PI3K, AKT, mTOR across various groups.

Table 3
Stability and repeatability results of the LC-MS.

t_R_m/z (min_Da)	Precision (RSD %)		System stability (RSD %)		Repeatability (RSD %)		Post-preparative stability (RE %)		Freeze–thaw Stability (RE %)	
	t_R	Area	t_R	Area	t_R	Area	t_R	Area	t_R	Area
1.6_262.8	0.7	6.5	0.5	10.9	0.2	7.3	0.3	−5.8	0.1	3.3
1.7_174.0	0.3	5.6	0.4	4.0	0.5	9.4	0.7	11.3	0.5	−7.9
2.24_160.2	0.8	8.1	0.4	3.9	0.3	10.3	0.5	−4.5	1.1	6.4
4.3_117.3	0.7	8.9	0.6	11.7	0.9	10.5	0.8	8.5	1.2	5.7
6.6_578.1	1.5	10.9	0.6	5.8	1.2	8.5	0.9	−4.0	1.4	7.5
8.6_244.2	0.6	8.1	0.6	7.9	1.4	13.9	1.1	8.4	0.9	−7.9

strong explanatory and predictive capabilities of the model. Additionally, the model was validated using a permutation test, where the Q^2 intercept on the y-axis should not exceed 0.05. The results of this test are presented (Table 4), showing that the Q^2 intercept values were all negative, confirming that the model is not overfitted. The permutation test results are depicted (Fig. 6c).

Metabolites with significant contributions to intergroup differences were selected as potential biomarkers based on the criteria of VIP > 1.0 and $p < 0.05$ from the Student's *t*-test. These biomarkers were subsequently identified using mass spectrometry data, literature references, and online database searches. A total of 22 differential metabolites were identified, as detailed (Table 4). The content changes of these metabolites were quantified based on the magnitude of the corrected peak areas, normalized by the internal standard. The integrated results of the content alterations of the identified metabolites are presented (Table 5).

3.7.7. Metabolic pathway analysis

Twenty-two potential biomarkers were imported into MetaboAnalyst 6.0 for metabolic pathway analysis. Pathways with strong associations were evaluated, and metabolic pathway impact maps were generated. Pathways with an impact score greater than 0.1 and a p-value less than 0.05 were considered potential key metabolic pathways. The results (Fig. 7A and Table 6) revealed five key metabolic pathways associated with the biomarkers, including: (a) arginine biosynthesis; (b) alanine, aspartic acid, and glutamic acid metabolism; (c) citric acid cycle (TCA cycle); (d) histidine metabolism; and (e) biosynthesis of phenylalanine, tyrosine, and tryptophan. Additionally, the 16 potential biomarkers related to the anti-tumor effects of XJZD were imported into MetaboAnalyst 6.0 for further pathway analysis. A total of six metabolic pathways were significantly associated with the anti-tumor effects of XJZD, which included: (a) alanine, aspartic acid, and glutamic acid metabolism; (b) citric acid cycle (TCA cycle); (c) histidine metabolism;

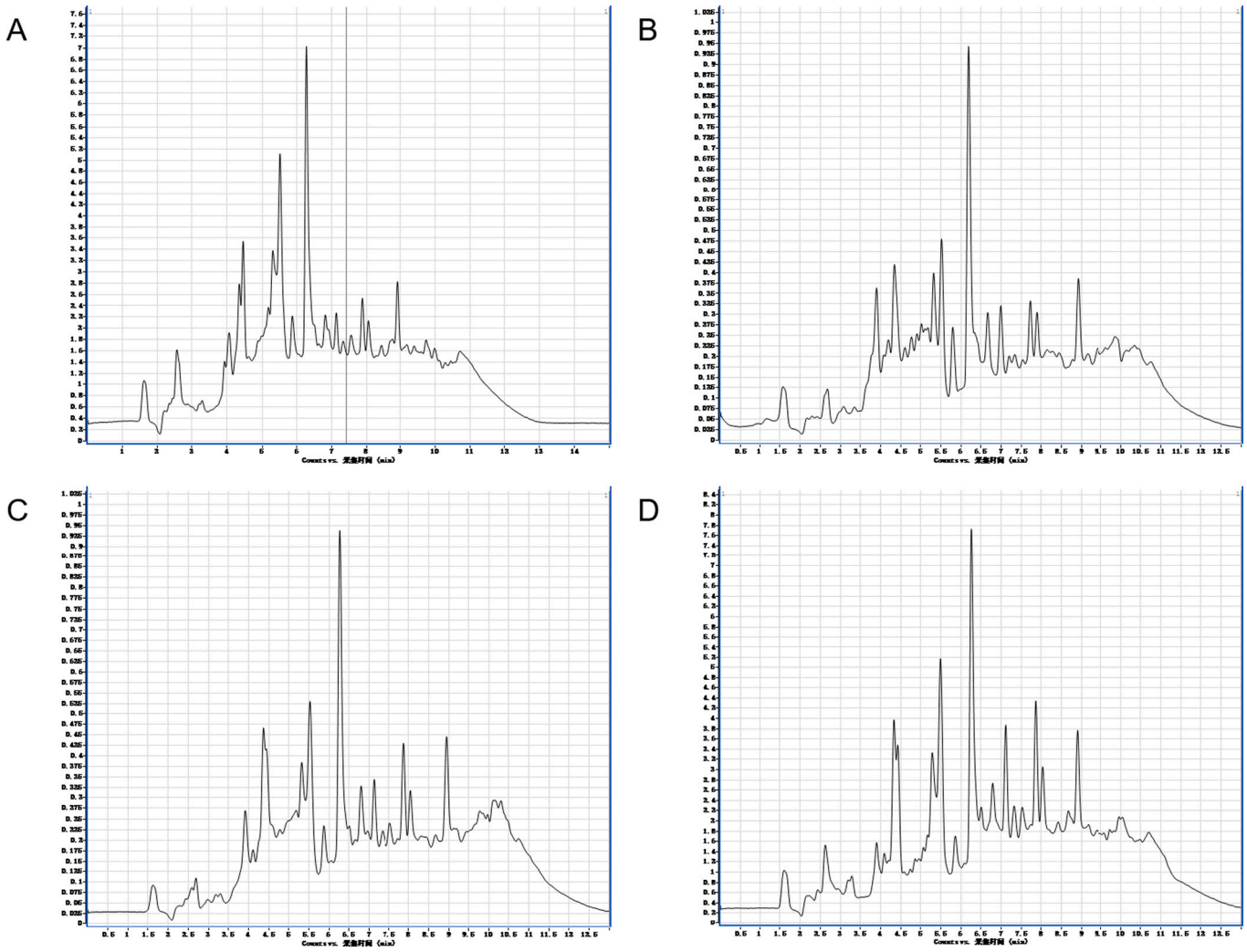

Fig. 5. Typical UPLC-MS TIC chromatograms of cells metabolite profiles. A: GC group, B: XJZD group, C: 5-Fu group, D: XJZD+5-Fu group.

(d) biosynthesis of phenylalanine, tyrosine, and tryptophan; (e) linoleic acid metabolism; and (f) tyrosine metabolism, as shown (Fig. 7B and Table 7).

4. Discussion

In this study, network pharmacology combined with network validation was initially employed to demonstrate that XJZD acts as a synergistic agent with multiple components, multiple targets, and multiple pathways in the treatment of GC. We explored the potential mechanisms by which XJZD influences GC and identified key active components and target proteins. The active constituent-target network of XJZD comprised 113 active constituents and 69 targets, highlighting the pharmacological foundation of XJZD. Surgery remains the only potentially curative treatment for early-stage GC [23]. 5-Fu is a standard chemotherapeutic drug used in the treatment of GC, but the issue of drug resistance limits its clinical effectiveness. The development of resistance to 5-Fu is primarily attributed to the upregulation of thymidylate synthase expression [24] and alterations in the regulators of apoptosis [25], XJZD can modulate the expression of apoptosis-related proteins, thereby sensitizing cancer cells to 5-Fu-induced cytotoxicity [26].To enhance the efficacy of 5-Fu and reduce its toxic side effects [27], network pharmacology was utilized to investigate the mechanism of action of XJZD in GC treatment, and the pharmacodynamics of XJZD combined with 5-Fu were further validated through in vitro experiments. By integrating the results of protein-protein interaction (PPI) network analysis with molecular docking, the primary therapeutic targets of XJZD were identified as TP53, STAT3, AKT1, JUN, ESR1, and IL6, the Degree values are 62,50,40,36,32,30. TP53 is the most frequently mutated gene in GC and may serve as a critical biomarker for the diagnosis and screening of this disease [28]. GC patients with TP53 mutations often present with more aggressive disease and exhibit resistance to chemotherapy [29], The TP53 tumor suppressor gene plays a crucial role in maintaining genomic stability and facilitating DNA repair processes [30]. STAT3 is pivotal in regulating tumor growth and metastasis [31]. Its activation in GC is associated with a poorer prognosis and lower survival rates [32]. STAT3 can be phosphorylated to pSTAT3, which promotes the survival of GC cells and inhibits apoptosis [33]. AKT1, a serine/threonine protein kinase, is critical in the development of GC [34], Silencing AKT1 has been shown to reduce the proliferation of GC cells [35] and increase apoptosis both in vitro and in vivo [36]. JUN is a key component of the activator protein-1 (AP-1) transcription factor complex [37], and the persistent stability of c-Jun contributes to the pathological changes in the gastric mucosa [38]. ESR1 is a commonly mutated estrogen receptor, with mutations identified as contributing factors to drug resistance in GC [39]. Overexpression of ESR1 promotes cellular proliferation and invasion in GC cells [40], although it also acts as a potential tumor suppressor in some contexts of GC [39]. IL6, a cytokine involved in inflammation and immune responses [41], plays a significant role in the onset [42] and progression of various malignancies, including GC [43],

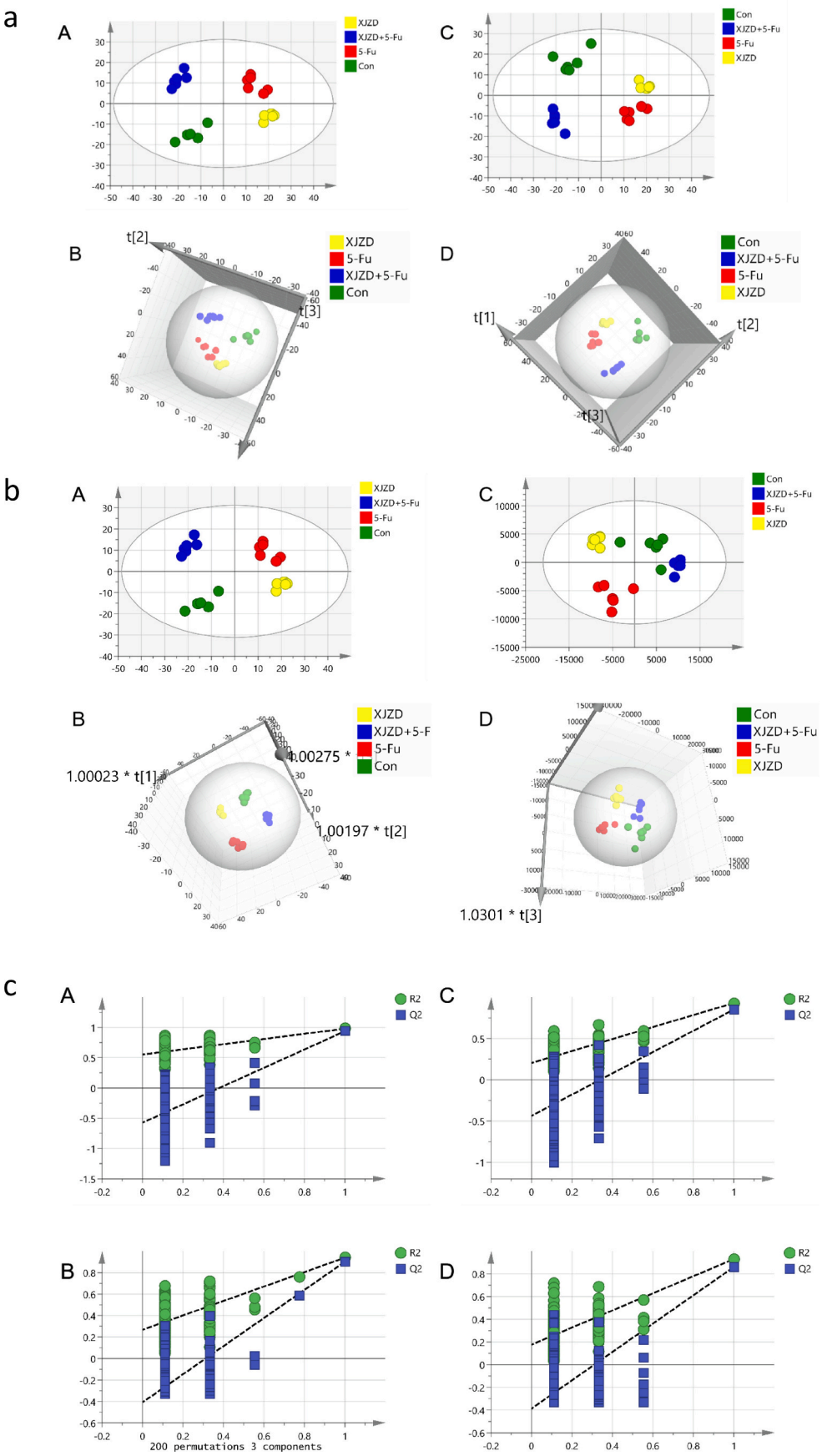

(caption on next page)

Fig. 6. a) Multivariate statistical analysis based on LC-MS. (A)Positive PCA Analysis, (B) Positive 3D-score graph, (C) negative PCA Analysis, (D) negative 3D-score graph. b) Multivariate statistical analysis based on LC-MS. Positive OPLS-DA Analysis (A), Positive 3D-score graph (B), negative OPLS-DA Analysis (C), negative 3D-score graph (D). c) Multivariate statistical analysis based on LC-MS. Positive Permutation tests of OPLS-DA models (A), Positive Permutation tests of PLS-DA models (B), negative Permutation tests of OPLS-DA models (C), negative Permutation tests of PLS-DA models (D).

Table 4
Difference markers.

tR(min)	m/z	Identification	Mode
1.594	268.2	Inosine	positive
1.704	174.24	D-alpha-Methyltryptamine	positive
2.198	115.1	Proline	positive
2.24	160.2	Tryptamine	positive
2.241	159.2	Stachydrine	positive
3.243	133.1	L-Aspartic acid	positive
4.244	257.2	Choline glycerophosphate	positive
4.311	189.2	L-Homocitrulline	positive
4.343	117.1	Betaine	positive
5.512	180.2	Inositol	positive
6.384	155.2	L-Histidine	positive
6.608	571.81	Taurocholic Acid	positive
6.946	175.2	L-Citruline	positive
7.653	257.2	5-Methylcytidine	positive
8.614	244.2	Uridine	positive
1.708	174.2	Linoleic acid	positive
2.284	192.1	Citric Acid	negative
3.955	173.2	N-Acetylleucine	negative
4.313	146.1	2-Ketoglutaric acid	negative
4.318	116.1	fumaric acid	negative
4.347	181.2	L-Tyrosine	negative
5.435	304.5	Arachidonic acid	negative

Table 5
Potential biomarkers detected by UPLC/MS and their changes between different groups.

Metabolites	XJZD/GC	5-Fu/GC	Com/5-Fu	Com/XJZD
Inosine	↑*		↑*	
D-alpha-Methyltryptamine	↓*	↓*	↓*	↓*
Proline	↑**	↑*		↑**
Tryptamine		↓**	↓**	↓*
Stachydrine	↓**	↓*	↓*	↓*
L-Aspartic acid	↓***	↓**		
Choline glycerophosphate		↓*	↓*	↓*
L-Homocitrulline	↓***		↓***	
Betaine	↑**	↑**		↑**
Inositol		↑**	↑*	↑**
L-Histidine	↑*	↑*	↑*	
Taurocholic Acid	↑***	↑*	↑**	↑*
L-Citruline		↑*		↑*
5-Methylcytidine		↓*		↓*
Uridine	↑**	↑**	↑*	
Linoleic acid	↓**	↓**	↓**	↓*
Citric Acid	↓***	↓**	↓*	
N-Acetylleucine		↓**	↓*	↓*
2-Ketoglutaric acid	↓*		↓*	
fumaric acid	↓**	↓***	↓*	↓**
L-Tyrosine	↓*		↓*	
Arachidonic acid	↑**	↑**	↑**	↑*

"↑" and "↓" means the metabolite was up-regulated and down-regulated. Significant difference compared with the GC group,"Com/5-Fu" refers to the combination treatment group compared to the 5-Fu group; "Com/XJZD" refers to the combination treatment group compared to the XJZD group, *P < 0.05, **$P < 0.01$, ***P < 0.

it was to play a role in the onset and progression of various malignant tumors [44], Recent studies have shown that circBGN promotes the growth and invasion of GC cells by activating the IL6/STAT3 signaling pathway [45]. Database validation further indicated that the levels of TP53, CCND1, MYC, and CTNNB1 were lower in GC tissues compared to normal tissues, suggesting their potential as significant biomarkers for the diagnosis and treatment of GC.

Our analysis indicates that the primary constituents of XJZD are quercetin, kaempferol, licochalcone A, beta-sitosterol, and naringenin. Among them, quercetin, kaempferol, and licochalcone A mainly exert therapeutic effects on gastric cancer through the PI3K/Akt signaling pathway, while beta-sitosterol and naringenin primarily act via the MAPK signaling pathway [46]. Quercetin has been shown to promote apoptosis in GC cells and exhibits anti-proliferative and anti-*Helicobacter pylori* activities [47]. Kaempferol reduces G2/M cyclin expression in GC, thereby inhibiting tumor cell growth [48]. Licochalcone A increases Rb expression and decreases the levels of cyclin A and cyclin B. Apoptosis induced by licochalcone A is associated with the regulation of PARP, caspase-3, Bcl-2, and Bax, thereby suppressing GC cell growth [49]. Beta-sitosterol has demonstrated pro-apoptotic, anti-proliferative, anti-metastasis, anti-invasion, and chemosensitizing effects on tumor cells [50]. Naringenin modulates beta-catenin/Tcf signaling in GC cells [51], inhibits Akt activation, and enhances p53 expression to inhibit gastric cell growth [52]. In summary, the studies reviewed here provide compelling evidence that XJZD, a traditional Chinese medicine formulation, contains key active components that exert significant inhibitory effects on GC.

GO enrichment analysis revealed that biological processes such as response to inorganic substances, positive regulation of protein phosphorylation, and related signaling pathways are directly implicated in the treatment of GC. The processes of adding and removing phosphate groups from tyrosine residues [53], carried out by protein tyrosine kinases and phosphatases (PTPs), are essential for cellular signal transduction [54] and play a crucial role in the regulation of gastric GC development [39].

Results from enrichment analysis revealed that the core therapeutic targets of XJZD primarily interact with key signaling pathways, including the MAPK, PI3K-Akt, and TNF signaling pathways. The mitogen-activated protein kinase (MAPK) pathways are crucial for regulating various cellular processes that drive the cancerous transformation of normal cells [21]. These pathways are widely conserved across multicellular organisms [55] and play pivotal roles in biological processes such as cell proliferation, apoptosis, differentiation, migration, and invasion [56]. However, network pharmacology studies are limited by the incompleteness of current databases, the potential inaccuracy of target prediction algorithms, and the lack of consideration for complex biological contexts, pharmacokinetics, and dynamic regulatory networks [57]. Therefore, we used cell experiments to validate the network pharmacology results. Our findings indicate that XJZD combined with 5-Fu significantly increased the mRNA levels of JNK1, JNK2 while significantly reducing the mRNA levels of ERK1, ERK2 and p38 in GC-803 cells. Studies have shown that DHA induces apoptosis in BGC-823 cells by activating the JNK1/2 MAPK signaling pathways [58]. Additionally, TSPAN8 has been reported to enhance tumor growth and metastasis, at least partially, by activating the ERK MAPK pathway [59]. This suggests that the combined treatment of XJZD and 5-Fu inhibits GC cell proliferation through modulation of the MAPK signaling pathway. The PI3K/AKT pathway is a critical signaling cascade downstream of many growth factor receptors and is one of the most prominent pathways involved in the progression of human cancers. It promotes tumor cell proliferation and malignant transformation while inhibiting apoptosis [22]. Targeting the PI3K pathway has been shown to drive cancer progression, partially via the MAPK signaling pathway [60]. Disruption of the PI3K-AKT-mTOR signaling pathway leads to inhibition of cancer growth [60]. In our study, we observed that XJZD combined with 5-Fu targeted the PI3K-AKT pathway in GC-803 cells, reducing the expression levels of PI3K, AKT, and mTOR, thus inhibiting the growth of

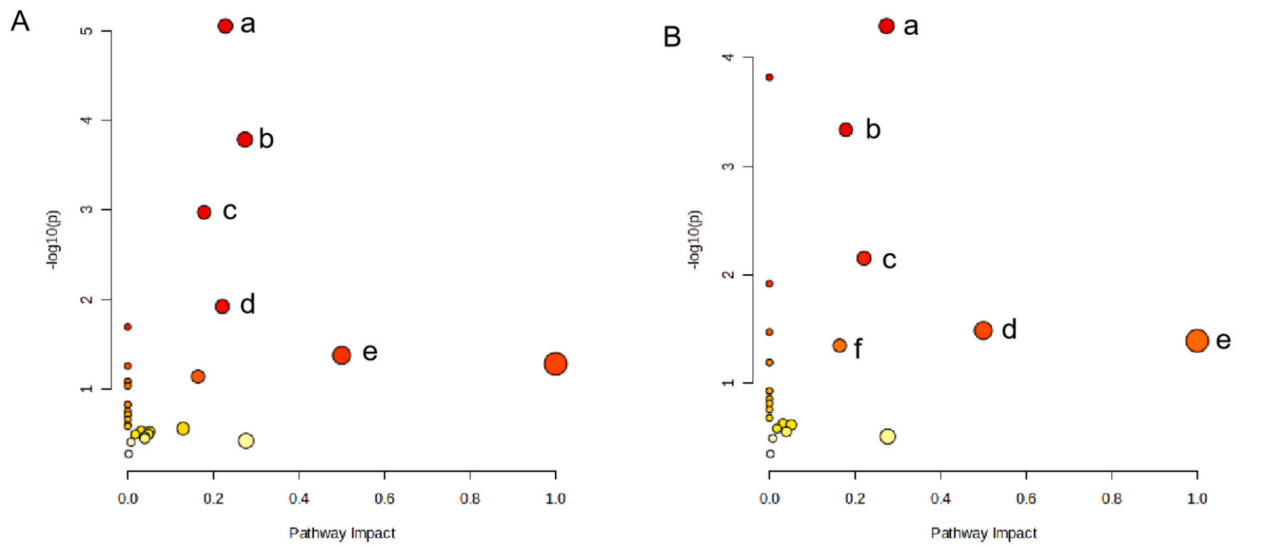

Fig. 7. (A) Meaningful pathways analysis based on key biomarkers ($P < 0.05$, impact-value>0.1), (B) Meaningful pathways analysis based on XJZD key biomarkers ($P < 0.05$, impact-value>0.1).

Table 6
Metabolic pathways.

Pathway Name	Match Status	P	Impact
Arginine biosynthesis	4/14	0.00001	0.22843
Alanine, aspartate and glutamate metabolism	4/28	0.00016	0.27404
Citrate cycle (TCA cycle)	3/20	0.00106	0.17875
Histidine metabolism	2/16	0.01204	0.22131
Phenylalanine, tyrosine and tryptophan biosynthesis	1/4	0.04252	0.5

Table 7
Metabolic pathways of XJZD.

Pathway Name	Match Status	P	Impact
Alanine, aspartate and glutamate metabolism	4/28	0.00005	0.27404
Citrate cycle (TCA cycle)	3/20	0.00046	0.17875
Histidine metabolism	2/16	0.00707	0.22131
Phenylalanine, tyrosine and tryptophan biosynthesis	1/4	0.03264	0.5
Linoleic acid metabolism	1/5	0.04065	1
Tyrosine metabolism	2/42	0.04496	0.16435

GC cells. TNF-alpha, a cytokine involved in various physiological and pathological processes such as cellular proliferation, differentiation, apoptosis, and regulation of immune responses, plays a significant role in the pathogenesis of cancer [61]. Polymorphisms in the TNF-alpha gene have been associated with an increased risk of developing GC and TNF-α/TNFR1 signaling contributes to tumor formation by stimulating the expression of Noxo1 and Gna14 in cancer cells. Our research suggests that XJZD may promote healing of GC by modulating these critical signaling pathways. Molecular docking studies revealed that beta-sitosterol exhibits a strong docking affinity with JUN, a core target within the anti-gastric cancer network. To validate the findings from the network pharmacology analysis and further elucidate the underlying mechanisms, we conducted in vitro experiments to confirm the therapeutic effects of XJZD on GC.

Through MTT assays, we found that XJZD combined with 5-Fu inhibited the proliferation of GC-803 cells in a dose-dependent manner, with the combined treatment showing enhanced efficacy. Apoptosis, a form of programmed cell death, is induced in response to both intrinsic and extrinsic signals [2]. Apoptosis serves as a crucial defense mechanism against cancer development and is an essential component of anticancer therapies [62]. Cellular metabolomics analysis indicates that the drug primarily exerts its effects by modulating the levels of tryptophan, betaine, or taurocholic acid, tryptamine, a product of tryptophan metabolism, has been reported to modulate cell proliferation and apoptosis through serotonin receptor signaling pathways [63], which are implicated in gastric cancer progression [64]. Betaine is involved in methylation reactions and has been shown to influence cell proliferation and apoptosis by regulating homocysteine metabolism and epigenetic modifications [65]. Taurocholic acid, a bile acid, can activate signaling pathways such as TGR5 [66], which have been linked to cancer cell proliferation and apoptosis. To further investigate the metabolic mechanisms underlying the action of XJZD combined with 5-Fu in GC, we analyzed key metabolic processes, including amino acid metabolism, energy metabolism, and related pathways.

Metabolomic analysis of amino acids has emerged as a promising approach for cancer screening [67]. Our results suggest that GC cells may be strongly dependent on certain amino acid metabolic pathways (e.g., alanine, aspartic acid, and glutamic acid metabolism) or enhanced glycolytic flux, which could represent promising therapeutic targets. Tumor cells can manipulate arginine metabolism to inhibit immune cell activity, which affects the growth and proliferation of NK cells and T cells, thereby creating an immunosuppressive tumor microenvironment that facilitates immune evasion [68]. In GC tissues, the aspartic acid levels were significantly higher than in normal gastric tissues [69]. The down-regulation of aspartic acid after drug treatment suggests a disturbance in this metabolic pathway. Histidine plays a role in regulating protein composition and the nervous system, and it also has protective effects, including intracellular pH stabilization and anti-inflammatory and antioxidant activities [70]. Histidine's anti-inflammatory effects are associated with the NF-κB and PPAR pathways, where it can inhibit NF-κB activation and reduce the production of pro-inflammatory cytokines [71]. The intermediates of the citric acid cycle (TCA cycle), such as citric acid, α-ketoglutaric acid, and fenugreek acid, play a critical role in cellular metabolism. The TCA cycle is a key source of anabolic precursors and is essential for basal cellular functions. Dysregulation of the TCA cycle is linked to the development of various

diseases, including tumors [72]. In cells treated with XJZD and 5-Fu, the levels of these TCA cycle intermediates were reduced, indicating a suppression of the TCA cycle. This suggests that the drug may interfere with mitochondrial enzyme activity, blocking the TCA cycle and disrupting energy replenishment, thus accelerating apoptosis and necrosis in cancer cells. Arginine has been shown to promote apoptosis by inhibiting the PI3K/Akt signaling pathway, specifically by upregulating the expression of cleaved Caspase-3 and Bad proteins [73]. Arginine is one of the three amino acids that can directly activate the mTOR signaling pathway, a crucial regulator of GC development [74]. This pathway's involvement suggests that arginine may influence GC progression by modulating mTOR signaling, providing a therapeutic target in clinical treatments for GC [75]. Moreover, energy metabolism is tightly connected to the MAPK pathway. Activation of MAPK14 under nutrient deprivation increases the expression of SLC2A3 (GLUT3), which enhances glucose uptake [76]. In vivo and in vitro studies have shown that chicory inulin can improve glucolipid metabolism by activating IRS and inhibiting the MAPK pathway [77]. Additionally, the activation of the JNK pathway influences insulin sensitivity, leading to altered enzyme activities that increase glycogenolysis and gluconeogenesis, further linking energy metabolism to cancer progression [78]. Consistent with the findings that MAMA decoction enhances the antimalarial efficacy of amodiaquine in a murine malaria model through synergistic effects, the present study also investigated the underlying mechanisms by analyzing relevant molecular pathways [79]. Both herbal formulations demonstrated potentiating effects when used as adjuvants to chemotherapeutic agents, suggesting that herbal preparations can enhance the efficacy of chemotherapy through modulation of specific molecular targets. In addition, this study employed cellular metabolomics to systematically analyze the alterations in intracellular metabolites following drug treatment, thereby providing further insights into the underlying mechanisms of action.

5. Conclusion

Potential targets of XJZD for the treatment of GC were identified through a combination of network-based screening and computational docking simulations. In vitro experiments demonstrated that XJZD significantly inhibited GC progression, with enhanced effects observed when combined with 5-Fu. This therapeutic effect was may be mediated through the modulation of the MAPK and PI3K-Akt signaling pathways, which play key roles in cell growth and survival. Further analysis of metabolic pathways revealed that XJZD exerts its effects primarily by influencing glycolysis, amino acid metabolism, and other related metabolic processes, thereby regulating the MAPK and PI3K-Akt signaling pathways to exert its therapeutic action against GC.

CRediT authorship contribution statement

Yanxue Xu: Writing – original draft, Methodology, Formal analysis, Conceptualization. **Yumeng Zhang:** Writing – review & editing, Validation, Funding acquisition. **Chen Huang:** Software, Data curation. **Min Zhao:** Supervision, Resources, Project administration, Funding acquisition. **Yihe Huang:** Supervision, Project administration.

Declaration of competing interest

The authors declare that they have no known competing financial interests or personal relationships that could have appeared to influence the work reported in this paper.

Acknowledgements

This work was supported by the Independent Topic Selection Project of Liaoning Provincial Department of Science and Technology (2023JH2/101600013) and the Basic Research Project (General Project) of Liaoning Provincial Department of Education (JYTMS20231376) and the Independent Topic Selection Project of Liaoning Provincial Department of Education (LJ212410163031).

Appendix A. Supplementary data

Supplementary data to this article can be found online at https://doi.org/10.1016/j.jchromb.2025.124671.

Data availability

Data will be made available on request.

References

[1] K. Jiang, H. Liu, J. Ge, B. Yang, Y. Wang, W. Wang, Y. Wen, S. Zeng, Q. Chen, J. Huang, X. Xiong, A study related to the treatment of gastric cancer with Xiang-Sha-Liu-Jun-Zi-Tang based on network analysis, Heliyon 9 (2023).
[2] J. Gao, S. Yang, G. Xie, J. Pan, F. Zhu, Integrating network pharmacology and experimental verification to explore the pharmacological mechanisms of Aloin against gastric Cancer, Drug Des. Devel. Ther. 16 (2022) 1947–1961.
[3] X. Deng, Z. Li, R. Xiong, J. Liu, R. Liu, J. Peng, Y. Chen, X. Lei, X. Cao, X. Zheng, Z. Xie, G. Tang, FS-7 inhibits MGC-803 cells growth in vitro and in vivo via down-regulating glycolysis, Biomed. Pharm. = Biomed. Pharmacotherapie 109 (2019) 1659–1669.
[4] Y. Qu, X. Yang, J. Li, S. Zhang, S. Li, M. Wang, L. Zhou, Z. Wang, Z. Lin, Y. Yin, J. Liu, N. Wang, Y. Yang, K. Arunachalam, Network pharmacology and molecular docking study of Zhishi-Baizhu herb pair in the treatment of gastric Cancer, Evid. Based Complement. Alternat. Med. 2021 (2021) 1–18.
[5] F. Qi, A. Li, Y. Inagaki, J. Gao, J. Li, N. Kokudo, X.K. Li, W. Tang, Chinese herbal medicines as adjuvant treatment during chemo- or radio-therapy for cancer, Biosci. Trends 4 (2010) 297–307.
[6] J. Chen, J. Zhang, T. Chen, S. Bao, J. Li, H. Wei, X. Hu, Y. Liang, F. Liu, S. Yan, Xiaojianzhong decoction attenuates gastric mucosal injury by activating the p62/Keap1/Nrf2 signaling pathway to inhibit ferroptosis, Biomed. Pharmacother. 155 (2022).
[7] J. Chen, J. Zhang, T. Chen, S. Bao, J. Li, H. Wei, X. Hu, Y. Liang, F. Liu, S. Yan, Xiaojianzhong decoction attenuates gastric mucosal injury by activating the p62/Keap1/Nrf2 signaling pathway to inhibit ferroptosis, Biomed. Pharm. = Biomed. Pharmacotherapie 155 (2022) 113631.
[8] E. Abbasi, DOI https://doi.org/10.1101/2025.02.06.25321832 (2025).
[9] J.G.O. Neto, S.K. Boechat, J.S. Romão, C.C. Pazos-Moura, K.J. Oliveira, Treatment with cinnamaldehyde reduces the visceral adiposity and regulates lipid metabolism, autophagy and endoplasmic reticulum stress in the liver of a rat model of early obesity, J. Nutr. Biochem. 77 (2020).
[10] Z.-Q. Yan, J. Tan, K. Guo, L.-G. Yao, Phytotoxic mechanism of allelochemical liquiritin on root growth of lettuce seedlings, Plant Signal. Behav. 15 (2020).
[11] W. Wang, W. Gu, C. He, T. Zhang, Y. Shen, Y. Pu, Bioactive components of Banxia Xiexin decoction for the treatment of gastrointestinal diseases based on flavor-oriented analysis, J. Ethnopharmacol. 291 (2022).
[12] T.J. Herrman, V. Hoffmann, A. Muiruri, C. McCormick, Aflatoxin proficiency testing and control in Kenya, J. Food Prot. 83 (2020) 142–146.
[13] W. Peng, L. Chen, J. Liu, Celastrol inhibits gastric cancer cell proliferation, migration, and invasion via the FOXA1/CLDN4 axis, Toxicol. Res. 12 (2023) 392–399.
[14] D.P. Mansingh, S. Pradhan, D. Biswas, R. Barathidasan, H.R. Vasanthi, Palliative role of aqueous ginger extract onN-Nitroso-N-Methylurea-induced gastric Cancer, Nutr. Cancer 72 (2019) 157–169.
[15] Y. Liu, X. Qin, G. Wang, Role of Saccharum Granorum as a “principal drug” in a traditional chinese medicine formula against chronic atrophic gastritis rats, Pharmacogn. Mag. 16 (2020).
[16] M. Cheng, T. Li, E. Hu, Q. Yan, H. Li, Y. Wang, J. Luo, T. Tang, A novel strategy of integrating network pharmacology and transcriptome reveals antiapoptotic mechanisms of Buyang Huanwu decoction in treating intracerebral hemorrhage, J. Ethnopharmacol. 319 (2024) 117123.
[17] X. Wang, Z.-Y. Wang, J.-H. Zheng, S. Li, TCM network pharmacology: a new trend towards combining computational, experimental and clinical approaches, Chin. J. Nat. Med. 19 (2021) 1–11.
[18] Y.-F. Liu, N. Ai, A. Keys, X.-H. Fan, M.-J. Chen, Network pharmacology for traditional Chinese medicine research: methodologies and applications, Chinese Herbal Med. 7 (2015) 18–26.
[19] X. Lin, T. Yu, L. Zhang, S. Chen, X. Chen, Y. Liao, D. Long, F. Shen, Silencing Op18/stathmin by RNA interference promotes the sensitivity of nasopharyngeal carcinoma cells to Taxol and high-grade differentiation of Xenografted Tumours in nude mice, Basic Clin. Pharmacol. Toxicol. 119 (2016) 611–620.
[20] D.S. Wishart, Metabolomics for investigating physiological and pathophysiological processes, Physiol. Rev. 99 (2019) 1819–1875.
[21] M. Sinkala, P. Nkhoma, N. Mulder, D.P. Martin, Integrated molecular characterisation of the MAPK pathways in human cancers reveals pharmacologically vulnerable mutations and gene dependencies, Commun. Biol. 4 (2021).

[22] Y. Lu, L. Li, G. Wu, H. Zhuo, G. Liu, J. Cai, Effect of PI3K/Akt signaling pathway on PRAS40Thr246 phosphorylation in gastric Cancer cells, Iran. J. Public Health 48 (2019) 2196–2204.
[23] L. Yan, The journey of personalizing gastric cancer treatment, Chin. J. Cancer 35 (2016).
[24] H. Yang, Q. Li, X. Chen, M. Weng, Y. Huang, Q. Chen, X. Liu, H. Huang, Y. Feng, H. Zhou, M. Zhang, W. Pei, X. Li, Q. Fu, L. Zhu, Y. Wang, X. Kong, K. Lv, Y. Zhang, Y. Sun, M. Ma, Targeting SOX13 inhibits assembly of respiratory chain supercomplexes to overcome ferroptosis resistance in gastric cancer, Nat. Commun. 15 (2024) 4296.
[25] T. Suetsugu, R. Mori, M. Futamura, M. Fukada, H. Tanaka, I. Yasufuku, Y. Sato, Y. Iwata, T. Imai, H. Imai, Y. Tanaka, N. Okumura, N. Matsuhashi, T. Takahashi, K. Yoshida, Mechanism of acquired 5FU resistance and strategy for overcoming 5FU resistance focusing on 5FU metabolism in colon cancer cell lines, Oncol. Rep. 45 (2021).
[26] T. Chen, S. Bao, J. Chen, J. Zhang, H. Wei, X. Hu, Y. Liang, J. Li, S. Yan, Xiaojianzhong decoction attenuates aspirin-induced gastric mucosal injury via the PI3K/AKT/mTOR/ULK1 and AMPK/ULK1 pathways, Pharm. Biol. 61 (2023) 1234–1248.
[27] J. Yuan, S.U. Khan, J. Yan, J. Lu, C. Yang, Q. Tong, Baicalin enhances the efficacy of 5-fluorouracil in gastric cancer by promoting ROS-mediated ferroptosis, Biomed. Pharmacother. 164 (2023).
[28] R. Yu, T. Sun, X. Zhang, Z. Li, Y. Xu, K. Liu, Y. Shi, X. Wu, Y. Shao, L. Kong, TP53 co-mutational features and NGS-calibrated immunohistochemistry threshold in gastric Cancer, Onco Targets Ther 14 (2021) 4967–4978.
[29] K. Wang, Z. Gong, Y. Chen, M. Zhang, S. Wang, S. Yao, Z. Liu, Z. Huang, B. Fei, KDM4C-mediated senescence defense is a targetable vulnerability in gastric cancer harboring TP53 mutations, Clin. Epigenetics 15 (2023).
[30] J. Saffari-Chaleshtori, M.-A. Tabatabaiefar, P. Ghasemi-Dehkordi, E. Farokhi, M.-T. Moradi, M. Hashemzadeh-Chaleshtori, The lack of correlation between TP53 mutations and gastric cancer: a report from a province of Iran, Genetika 49 (2017) 235–246.
[31] J. He, X. Feng, Y. Liu, Y. Wang, C. Ge, S. Liu, Y. Jiang, Graveoline attenuates D-GalN/LPS-induced acute liver injury via inhibition of JAK1/STAT3 signaling pathway, Biomed. Pharm. = Biomed. Pharmacotherapie 177 (2024) 117163.
[32] H. Zheng, H. Hong, L. Zhang, X. Cai, M. Hu, Y. Cai, B. Zhou, J. Lin, C. Zhao, W. Hu, Nifuratel, a novel STAT3 inhibitor with potent activity against human gastric cancer cells, Cancer Manag. Res. 9 (2017) 565–572.
[33] J.-Y. Deng, STAT-3 correlates with lymph node metastasis and cell survival in gastric cancer, World J. Gastroenterol. 16 (2010).
[34] X.-M. Wan, X.-L. Zhou, Y.-J. Du, H. Shen, Z. Yang, Y. Ding, X.-J. Lu, TASP1 promotes proliferation and migration in gastric Cancer via EMT and AKT/P-AKT pathway, J Immunol Res 2021 (2021) 1–9.
[35] Y. Yan, B. Li, Q. Gao, M. Wu, H. Ma, J. Bai, C. Ma, X. Xie, Y. Gong, L. Xu, X. Li, W. Wang, Y. Wu, J. Wang, H. Wang, Y. Feng, Y. Zhang, P. Li, H. Shi, F. Ma, Y. Jia, H. Duan, X. Fu, W. Wang, L. Zhan, X. Du, H. Zhou, Y. Liao, Intestine-Decipher Engineered Capsules Protect Against Sepsis-induced Intestinal Injury via Broad-spectrum Anti-inflammation and Parthanatos Inhibition, Adv. Sci. (Weinheim, Baden-Wurttemberg, Germany) 12 (2025) e2412799.
[36] W. Zhou, X.-Q. Fu, J. Liu, H.-G. Yu, RNAi knockdown of the Akt1 gene increases the chemosensitivity of gastric cancer cells to cisplatin both in vitro and in vivo, Regul. Pept. 176 (2012) 13–21.
[37] Y. Zhang, W.-L. Shen, M.-L. Shi, L.-Z. Zhang, Z. Zhang, P. Li, L.-Y. Xing, F.-Y. Luo, Q. Sun, X.-F. Zheng, X. Yang, Z.-H. Zhao, Involvement of aberrant miR-139/Jun feedback loop in human gastric cancer, Biochimica et Biophysica Acta (BBA) - molecular, Cell Res. 1853 (2015) 481–488.
[38] D.H. Jin, J. Lee, K.M. Kim, S. Kim, D.H. Kim, J. Park, Overexpression of MAPK15 in gastric cancer is associated with copy number gain and contributes to the stability of c-Jun, Oncotarget 6 (2015) 20190–20203.
[39] L. Shang, X. Chen, T. Zhu, S. Chong, H. Liu, W. Huang, W. Fu, H. She, X. Shen, Cancer-associated fibroblast-secreted exosomes promote gastric Cancer cell migration and invasion via the IL-32/ESR1 Axis, Appl. Biochem. Biotechnol. (2025), https://doi.org/10.1007/s12010-023-04782-6(2024).
[40] J. Zhou, R. Teng, C. Xu, Q. Wang, J. Guo, C. Xu, Z. Li, S. Xie, J. Shen, L. Wang, Overexpression of ERα inhibits proliferation and invasion of MKN28 gastric cancer cells by suppressing β-catenin, Oncol. Rep. 30 (2013) 1622–1630.
[41] E. Abbasi, Investigating the role of vitamin D in the prevention and control of dengue virus vectors and related diseases: a systematic review study, Epidemiol. Rev. (2025), https://doi.org/10.1093/epirev/mxaf006(2025).
[42] K. Wang, J. Yin, J. Chen, J. Ma, H. Si, D. Xia, Inhibition of inflammation by berberine: molecular mechanism and network pharmacology analysis, Phytomedicine : international journal of phytotherapy and phytopharmacology 128 (2024) 155258.
[43] M. Liu, H. Li, H. Zhang, H. Zhou, T. Jiao, M. Feng, F. Na, M. Sun, M. Zhao, L. Xue, L. Xu, RBMS1 promotes gastric cancer metastasis through autocrine IL-6/JAK2/STAT3 signaling, Cell Death Dis. 13 (2022).
[44] G. Hou, H. Zuo, J. Shi, D. Dai, H. Wang, X. Song, G. Xu, G. Tao, EIF4A3 induced circABCA5 promotes the gastric cancer progression by SPI1 mediated IL6/JAK2/STAT3 signaling, Am. J. Cancer Res. 13 (2023) 602–622.
[45] C. Li, X. Peng, Z. Peng, B. Yan, circBGN accelerates gastric cancer cell proliferation and invasion via activating IL6/STAT3 signaling pathway, FASEB J. 36 (2022) e22604.
[46] E. Abbasi, S. Saeedi, DOI 10.21203/rs.3.rs-2104725/v1 (2022).
[47] A. Haghi, H. Azimi, R. Rahimi, A comprehensive review on Pharmacotherapeutics of three phytochemicals, curcumin, quercetin, and Allicin, in the treatment of gastric Cancer, journal of gastrointestinal, Cancer 48 (2017) 314–320.
[48] T. Singh, D. Sharma, R. Sharma, H.S. Tuli, S. Haque, S. Ramniwas, D.M. Mathkor, V. Yadav, The role of phytonutrient Kaempferol in the prevention of gastrointestinal cancers: recent trends and future perspectives, Cancers 16 (2024).
[49] X.-Y. Xiao, M. Hao, X.-Y. Yang, Q. Ba, M. Li, S.-J. Ni, L.-S. Wang, X. Du, Licochalcone a inhibits growth of gastric cancer cells by arresting cell cycle progression and inducing apoptosis, Cancer Lett. 302 (2011) 69–75.
[50] X. Bao, Y. Zhang, H. Zhang, L. Xia, Molecular mechanism of β-Sitosterol and its derivatives in tumor progression, Front. Oncol. 12 (2022).
[51] J.H. Lee, C.H. Park, K.C. Jung, H.S. Rhee, C.H. Yang, Negative regulation of β-catenin/Tcf signaling by naringenin in AGS gastric cancer cell, Biochem. Biophys. Res. Commun. 335 (2005) 771–776.
[52] H. Zhang, X.I.A. Zhong, X. Zhang, D. Shang, Y.I. Zhou, C. Zhang, Enhanced anticancer effect of ABT-737 in combination with naringenin on gastric cancer cells, Exp. Ther. Med. 11 (2016) 669–673.
[53] S. Chen, S. Long, Y. Liu, S. Wang, Q. Hu, L. Fu, D. Luo, Evaluation of a three-gene methylation model for correlating lymph node metastasis in postoperative early gastric cancer adjacent samples, Front. Oncol. 14 (2024) 1432869.
[54] E. Abbasi, Investigating the role of vitamin D in the prevention and control of dengue virus vectors and related diseases: a systematic review study, Epidemiol. Rev. (2025), https://doi.org/10.1093/epirev/mxaf006.
[55] E. Abbasi, Changing physician performance: a systematic review and Meta-analysis (75 years 1950-2024) of the effect of continuing medical education strategies, continuous professional development and knowledge translation, 2025, https://doi.org/10.1101/2025.02.06.25321832.
[56] M. Yang, Mitogen-activated protein kinase signaling pathway and invasion and metastasis of gastric cancer, World J. Gastroenterol. 21 (2015).
[57] C. Feng, Y. Wang, J. Xu, Y. Zheng, W. Zhou, Y. Wang, C. Luo, Precisely tailoring molecular structure of doxorubicin prodrugs to enable stable Nanoassembly, rapid activation, and potent antitumor effect, Pharmaceutics 16 (2024).
[58] Y. Zhang, M. Xu, X. Zhang, F. Chu, T. Zhou, MAPK/c-Jun signaling pathway contributes to the upregulation of the anti-apoptotic proteins Bcl-2 and Bcl-xL induced by Epstein-Barr virus-encoded BARF1 in gastric carcinoma cells, Oncol. Lett. (2025), https://doi.org/10.3892/ol.2018.8293(2018).
[59] L. Wei, Y. Li, Z. Suo, TSPAN8 promotes gastric cancer growth and metastasis via ERK MAPK pathway, Int. J. Clin. Exp. Med. 8 (2015) 8599–8607.
[60] D. Tewari, P. Patni, A. Bishayee, A.N. Sah, A. Bishayee, Natural products targeting the PI3K-Akt-mTOR signaling pathway in cancer: a novel therapeutic strategy, Semin. Cancer Biol. 80 (2022) 1–17.
[61] P. Mahdavi Sharif, P. Jabbari, S. Razi, M. Keshavarz-Fathi, N. Rezaei, Importance of TNF-alpha and its alterations in the development of cancers, Cytokine 130 (2020).
[62] H. Wang, T. Zhang, W. Sun, Z. Wang, D. Zuo, Z. Zhou, S. Li, J. Xu, F. Yin, Y. Hua, Z. Cai, Erianin induces G2/M-phase arrest, apoptosis, and autophagy via the ROS/JNK signaling pathway in human osteosarcoma cells in vitro and in vivo, Cell Death Dis. 7 (2016) e2247.
[63] T. Li, L. Zhang, M. Cheng, E. Hu, Q. Yan, Y. Wu, W. Luo, H. Su, Z. Yu, X. Guo, Q. Chen, F. Zheng, H. Li, W. Zhang, T. Tang, J. Luo, Y. Wang, Metabolomics integrated with network pharmacology of blood-entry constituents reveals the bioactive component of Xuefu Zhuyu decoction and its angiogenic effects in treating traumatic brain injury, Chin. Med. 19 (2024) 131.
[64] F. Abedini, O. Amjadi, G. Ahangari, Repurposing serotonergic drugs for gastric cancer: induction of apoptosis in vitro, Mol. Biol. Rep. 52 (2025) 373.
[65] X. Men, X. Shi, Q. Xu, M. Liu, H. Yang, L. Wang, X. Men, H. Xu, Exploring the pathogenesis of chronic atrophic gastritis with atherosclerosis via microarray data analysis, Medicine 103 (2024) e37798.
[66] A. Çakır Gündoğdu, F. Kar, C. Özbayer, Investigation of the Gastroprotective effect of betaine-homocysteine homeostasis on oxidative stress, inflammation and apoptosis in ethanol-induced ulcer model, J. Investigative Surgery : Off. J. Academy Surgical Res. 35 (2022) 1806–1817.
[67] K. Katayama, A. Higuchi, H. Yamamoto, A. Ikeda, S. Kikuchi, M. Shiozawa, Perioperative dynamics and significance of plasma-free amino acid profiles in colorectal cancer, BMC Surg. 18 (2018) 11.
[68] C. Li, M. Niu, R. Wang, X.W. Zhou, B. Dong, S. Qi, W. Chen, M. Zhang, Y. Shi, R. Li, G. Li, The modulatory properties of Si Jun Zi Tang enhancing anticancer of gefitinib by an integrating approach, Biomed. Pharm. = Biomed. Pharmacotherapie 111 (2019) 1132–1140.
[69] A. Okada, H. Takehara, K. Yoshida, M. Nishi, H. Miyake, Y. Kita, N. Komi, Increased aspartate and glutamate levels in both gastric and colon cancer tissues, Tokushima J. Exp. Med. 40 (1993) 19–25.
[70] R.N. Feng, Y.C. Niu, X.W. Sun, Q. Li, C. Zhao, C. Wang, F.C. Guo, C.H. Sun, Y. Li, Histidine supplementation improves insulin resistance through suppressed inflammation in obese women with the metabolic syndrome: a randomised controlled trial, Diabetologia 56 (2013) 985–994.
[71] A. Andou, T. Hisamatsu, S. Okamoto, H. Chinen, N. Kamada, T. Kobayashi, M. Hashimoto, T. Okutsu, K. Shimbo, T. Takeda, H. Matsumoto, A. Sato, H. Ohtsu, M. Suzuki, T. Hibi, Dietary histidine ameliorates murine colitis by inhibition of proinflammatory cytokine production from macrophages, Gastroenterology 136 (2009) 564–574.e562.
[72] J.J. Brière, J. Favier, A.P. Gimenez-Roqueplo, P. Rustin, Tricarboxylic acid cycle dysfunction as a cause of human diseases and tumor formation, Am. J. Phys. Cell Phys. 291 (2006) C1114–C1120.
[73] I. Horwacik, H. Rokita, Targeting of tumor-associated gangliosides with antibodies affects signaling pathways and leads to cell death including apoptosis, Apoptosis : Int. J. Programmed Cell Death 20 (2015) 679–688.
[74] D.T. Morgos, C. Stefani, D. Miricescu, M. Greabu, S. Stanciu, S. Nica, S. Stanescu II, D.G. Balan, A.E. Balcangiu-Stroescu, E.C. Coculescu, D.E. Georgescu, R.I. Nica,

Targeting PI3K/AKT/mTOR and MAPK signaling pathways in gastric Cancer, Int. J. Mol. Sci. 25 (2024).
[75] H. Ban, K. Shigemitsu, T. Yamatsuji, M. Haisa, T. Nakajo, M. Takaoka, T. Nobuhisa, M. Gunduz, N. Tanaka, Y. Naomoto, Arginine and leucine regulate p70 S6 kinase and 4E-BP1 in intestinal epithelial cells, Int. J. Mol. Med. 13 (2004) 537–543.
[76] W.H. Cao, Y. Xiong, Q.F. Collins, H.Y., Liu, p38 mitogen-activated protein kinase plays a critical role in the control of energy metabolism and development of cardiovascular diseases, Zhong nan da xue xue bao, Yi xue ban = J. Central South Univ. Med. Sci. 32 (2007) 1–14.
[77] C. Ning, X. Wang, S. Gao, J. Mu, Y. Wang, S. Liu, J. Zhu, X. Meng, Chicory inulin ameliorates type 2 diabetes mellitus and suppresses JNK and MAPK pathways in vivo and in vitro, Mol. Nutr. Food Res. 61 (2017).
[78] S.N. Vallerie, G.S. Hotamisligil, The role of JNK proteins in metabolism, Sci. Transl. Med. 2 (2010) 60rv65.
[79] L. Bin, Q. Gao, Y. Wu, H. Lei, S. Ma, W. Wang, H. Sun, W. Ma, J. Zheng, C. Yuan, Y. Zhang, Y. Jia, M. Ma, Q. Gu, S. Sang, H. Duan, H. Shi, X. Fu, G. Lu, Z. Shan, Y. Jiang, Y. Liao, Broad-spectrum anti-inflammatory and antioxidant therapy of inflammatory-storm actuated diseases via programmable self-derived cryo-dead neutrophils, Chem. Eng. J. 507 (2025) 160643.